J Eng Math (2022) 132:11
https://doi.org/10.1007/s10665-021-10190-8

Buoyancy-driven algebraic (localised) boundary-layer disturbances

S. M. Edwards · **R. E. Hewitt**

Received: 1 July 2021 / Accepted: 26 October 2021 / Published online: 16 December 2021

Abstract We show that a new class of steady linear eigenmodes exist in the Falkner–Skan boundary layer, associated with an algebraically developing, thermally coupled three-dimensional perturbation that remains localised in the spanwise direction. The dominant mode has a weak temperature difference that decays (algebraically) downstream, but remains sufficient (for favourable pressure gradients that are below a critical level) to drive an algebraically growing disturbance in the velocity field. We determine the critical Prandtl number and pressure gradient parameter required for downstream algebraic growth. We also march the nonlinear boundary-region equations downstream, to demonstrate that growth of these modes eventually gives rise to streak-like structures of order-one aspect ratio in the cross-sectional plane. Furthermore, this downstream flow can ultimately become unstable to a two-dimensional Rayleigh instability at finite amplitudes.

Keywords Boundary-layer · Buoyancy · High-Reynolds number · Inviscid stability

1 Introduction and formulation

Algebraically developing (two-dimensional) disturbance modes in a flat-plate boundary layer were described in the early work of Libby and Fox [1] and Stewartson [2]. For a dimensionless downstream coordinate x, with leading edge at $x = 0$ and transverse coordinate y these two-dimensional flows are described by the stream function

$$\varphi(x, Y) = (2x)^{1/2}\{F(\eta) + \epsilon x^{\lambda} f(\eta)\}, \quad \text{with} \quad \eta = Y/(2x)^{1/2}, \tag{1}$$

where $\epsilon \ll 1$ is the disturbance amplitude, Y is the boundary-layer coordinate $Y = y\,\mathrm{Re}^{1/2}$ and $\mathrm{Re} \gg 1$ a Reynolds number. Here F satisfies the Blasius ordinary-differential equation

$$F'''(\eta) + F(\eta)F''(\eta) = 0, \quad F(0) = F'(0) = 0, \quad F'(\infty) = 1. \tag{2}$$

A one-dimensional eigenvalue problem is obtained for the disturbance shape $f(\eta)$ and eigenvalue λ. Libby and Fox showed that such modes decay downstream with $\lambda \leq -1$; Stewartson had already showed that a disturbance with $\lambda = -1$ can be found explicitly, which turns out to be the slowest decaying two-dimensional disturbance for the Blasius boundary layer. Although the focus of the Libby and Fox analysis was on providing a perturbation

S. M. Edwards (✉)· R. E. Hewitt
Department of Mathematics, University of Manchester, Manchester M13 9PL, UK
e-mail: sean.edwards@manchester.ac.uk

approximation to the downstream solution, it should be noted that the self-similar form of (1) applies globally at all downstream locations.

The two-dimensional Blasius problem was subsequently extended to a mixed-convection boundary layer, both with and without an externally applied pressure gradient. This extension proved to be non-trivial and has some peculiar properties that were the root cause of confusion in the early literature, particularly for the boundary-layer flow above a cold surface as described by Schneider and Wasel [3], Wickern [4,5] and Daniels [6]. These inconsistent results were ultimately clarified by the local analysis of Steinrück [7], who showed that two-dimensional disturbances grow downstream with a growth rate that becomes unbounded. This susceptibility to what may be thought of as short-scale perturbations causes significant issues to numerical procedures for downstream marching of the parabolic governing equations for two-dimensional mixed-convection boundary layers.

The Steinrück analysis took a local parallel flow approach to describe the disturbance field, which can be justified in the limit of unbounded downstream spatial growth. However, a more general approach was later presented by Denier et al. [8] by an examination of algebraic modes of the form (1) extended to include a temperature field and assuming a Grashof number of $O(\mathrm{Re}^{5/2})$ in terms of a Reynolds number Re. For positive Grashof numbers (a heated surface), the eigenvalue problem was solved to show that $\lambda < 0$ (decaying relative to the base flow) in the absence of pressure gradients. In the forced-convection limit the Libby and Fox [1] eigenvalues of (1) still apply, but there is now a slower-decaying ($\lambda \approx -0.296$ for a Prandtl number $\mathrm{Pr} \approx 0.7$) disturbance associated primarily with the energy equation. For negative Grashof numbers (a cooled surface), growing $\lambda > 0$ disturbances are recovered which, in agreement with the observations of Steinrück [7], become unbounded ($\lambda \to \infty$) as the scaled Grashof number approaches zero from below (with no external pressure gradient). These infinite growth-rate 'short-scale' waves owe their presence to the large Grashof number ($\mathrm{Gr} \sim \mathrm{Re}^{5/2}$) and the resultant coupling with a streamwise pressure gradient. They effectively render the parabolic two-dimensional mixed-convection problem ill-posed. Denier et al. demonstrated that short-scale perturbations can be suppressed by specifying Neumann conditions at the downstream boundary coupled with a quasi-elliptic approach to the computations. However, for three-dimensional disturbances (as we shall discuss here) a buoyancy coupling is achieved with a weaker thermal forcing ($\mathrm{Gr} \sim \mathrm{Re}^{3/2}$), and this recovers a well-posed parabolic problem.

Additional extensions of (1) to capture three-dimensional disturbances were introduced by Luchini [9] by assuming spanwise periodicity for the isothermal Blasius boundary layer whilst similar descriptions were used by Duck et al. [10] in the context of isothermal corner boundary layers. The corresponding analysis presented by Luchini is inevitably local in nature, owing to the transverse length scale of the flow (the boundary-layer thickness) typically growing downstream in contrast to any assumed fixed spanwise wavelength of the disturbance field. However, as recently shown by Hall [11] the Luchini modes dominate at the leading edge, where the spanwise wavelength is large (relative to the transverse scale). These disturbances then describe a locally self-similar near wall response that grows as $x^{0.223}$, with an outer non-self-similar layer that acts to reduce the transverse flow to zero, before developing directly into unstable Görtler vortices.

An alternative global approach to three-dimensional disturbances has recently been formulated by Hewitt and Duck [12], by assuming a spanwise length scale that remains commensurate with the transverse scale, both developing in tandem downstream [13]. In this new approach, there is spanwise diffusion and the disturbance ultimately decays in the far-spanwise direction, remaining localised (rather than periodic). It is possible to construct linearised self-similar disturbances relevant to all downstream locations by extending the form of (1) to give a velocity field of

$$\begin{aligned}(u, v, w) = &\left(F'(\eta),\ (2x)^{-1/2}[\eta F'(\eta) - F(\eta)],\ 0\right)\\ &+ \epsilon x^{\lambda}(u(\eta,\zeta), v(\eta,\zeta), w(\eta,\zeta)), \quad \text{with} \quad (\eta,\zeta) = (Y, Z)/(2x)^{1/2},\end{aligned} \tag{3}$$

where (u, v, w) are the streamwise, transverse and spanwise velocity components with $(y, z) = (Y, Z)\mathrm{Re}^{-1/2}$ and Z is the spanwise coordinate. In this approach, localised three-dimensional modes are found to decay relative to the base flow with $\lambda \approx -0.787$ when F is the corresponding Blasius solution of (2).

In this work, we return to the downstream development of three-dimensional disturbances in the form of (3) applied to a horizontal boundary layer, but include thermal effects leading to a buoyancy coupling with the transverse momentum. In addition, we extend the base flow from Blasius to the Falkner–Skan [14] boundary layer, where the inviscid (outer) flow is assumed to have a dimensional streamwise velocity $U_\infty^* x^n$, where $n > 0$ is associated with a favourable external pressure gradient.

Away from any bounding surface we consider an incompressible fluid of known reference temperature T_∞^* and density ρ_∞^*, but allow for temperature variations of magnitude ΔT^* within the boundary layer. For a reference length scale of L^*, we consider the high Reynolds number regime, with

$$\mathrm{Re} = \frac{L^* U_\infty^*}{\nu^*} \gg 1, \tag{4}$$

for a constant kinematic viscosity ν^*. The appropriate perturbation expansions for the dimensionless coordinates, velocities, temperature and pressure (respectively) are

$$(y, z) = \mathrm{Re}^{-\frac{1}{2}}(Y, Z), \tag{5a}$$

$$(u, v, w) = (\hat{U}(x, Y, Z), \mathrm{Re}^{-\frac{1}{2}}\hat{V}(x, Y, Z), \mathrm{Re}^{-\frac{1}{2}}\hat{W}(x, Y, Z)) + \cdots, \tag{5b}$$

$$T = \hat{\vartheta}(x, Y, Z) + \cdots, \tag{5c}$$

$$p = -\frac{1}{2}[u_e(x)]^2 + \mathrm{Re}^{-\frac{1}{2}} p_1(x) + \mathrm{Re}^{-1}\hat{P}(x, Y, Z) + \cdots, \tag{5d}$$

where $u_e(x) = x^n$. Under a Boussinesq approximation with gravity in the $-Y$ direction, the leading-order (steady) equations take the form

$$\hat{U}_x + \hat{V}_Y + \hat{W}_Z = 0, \tag{6a}$$

$$\hat{U}\hat{U}_x + \hat{V}\hat{U}_Y + \hat{W}\hat{U}_Z = u_e(x)u_e'(x) + \hat{U}_{YY} + \hat{U}_{ZZ}, \tag{6b}$$

$$\hat{U}\hat{V}_x + \hat{V}\hat{V}_Y + \hat{W}\hat{V}_Z = -\hat{P}_Y + \hat{V}_{YY} + \hat{V}_{ZZ} + \mathrm{G}\,\hat{\vartheta}, \tag{6c}$$

$$\hat{U}\hat{W}_x + \hat{V}\hat{W}_Y + \hat{W}\hat{W}_Z = -\hat{P}_Z + \hat{W}_{YY} + \hat{W}_{ZZ}, \tag{6d}$$

$$\hat{U}\hat{\vartheta}_x + \hat{V}\hat{\vartheta}_Y + \hat{W}\hat{\vartheta}_Z = \frac{1}{\mathrm{Pr}}(\hat{\vartheta}_{YY} + \hat{\vartheta}_{ZZ}), \tag{6e}$$

subject to $\hat{U} = \hat{V} = \hat{W} = 0$ and $\hat{\vartheta}$ prescribed on the surface ($Y = 0$), with $\hat{U} \to u_e(x)$, $\hat{\vartheta} \to 0$ and $\hat{W} \to 0$ as $Y \to \infty$. Here, we have assumed an $O(\mathrm{Re}^{3/2})$ Grashof number and an $O(1)$ Prandtl number, such that

$$\mathrm{Gr} = \frac{\Delta T^* \alpha^* g^* L^{*3}}{\nu^{*2}} = \mathrm{Re}^{3/2}\mathrm{G}, \quad \mathrm{Pr} = \frac{\mu^* c_p^*}{\kappa^*}, \tag{7}$$

with constant specific heat c_p^*, thermal conductivity κ^*, thermal expansion coefficient α^* and gravitational acceleration g^*.

In the absence of any localised thermal forcing or instability, a self-similar two-dimensional ($\hat{W} \equiv 0$) solution can be found to (6) in Falkner–Skan [14] form as follows:

$$\hat{U}(x, Y) = x^n F'(\eta), \quad \hat{V}(x, Y) = \left(\frac{n+1}{2}\right)^{\frac{1}{2}} x^{\frac{n-1}{2}}\left[\frac{1-n}{1+n}\eta F'(\eta) - F(\eta)\right], \quad \hat{\vartheta}(x, Y) = x^{\frac{3(n-1)}{2}} H(\eta), \tag{8a}$$

where

$$\eta = \left(\frac{n+1}{2}\right)^{\frac{1}{2}} x^{\frac{n-1}{2}} Y. \tag{8b}$$

Here, $F(\eta)$ and $H(\eta)$ are determined from the Falkner–Skan equation and coupled energy equation

$$F''' + FF'' + \beta(1 - F'^2) = 0, \quad F(0) = F'(0) = 0, \quad F'(\infty) = 1, \tag{8c}$$

$$H'' + \mathrm{Pr}\, FH' + 3\mathrm{Pr}\,(1-\beta)F'H = 0, \quad H(0) = H_w, \quad H(\infty) = 0, \tag{8d}$$

parameterised in terms of the Hartree [15] parameter $\beta = 2n/(n+1)$. Here, H_w is a dimensionless boundary temperature, which by choice of ΔT^* can be set to unity; however, here we will later consider the case of $H_w = 0$ (so $H \equiv 0$ and there is only a spatially localised temperature difference).

The downstream ($x^{3(n-1)/2}$) form of the temperature is chosen to retain the buoyancy coupling in the three-dimensional problem, but this is only appropriate for $\mathrm{G} = O(1)$. If $\mathrm{G} = O(\mathrm{Re})$ then there is additional coupling between the temperature field and the streamwise momentum equation via the downstream pressure gradient, in which case we would require surface temperature differences proportional to $x^{(5n-1)/2}$ instead, as considered by Denier et al. [8] amongst others. Throughout this discussion we assume that $\mathrm{G}/\mathrm{Re} = o(1)$, which avoids any growth of short-scale perturbations of the form described by [8].

If we instead choose a uniform heated plate, we recover the non-self-similar formulation of Hall and Morris [16] who showed that linear disturbances typically decay from an initiation site, before starting to grow further downstream as the flow becomes unstable to longitudinal vortex modes. The description of [16] is the most generic way for vortex modes to be generated in the presence of surface heating over spanwise scales that are large compared to the boundary-layer thickness.

Here, we extend the decomposition (3) (and therefore (1)) to include a temperature field and bouyancy coupling in the context of (6). Section 2 solves the resulting bi-global (linear) eigenvalue problem to obtain a disturbance field that grows algebraically like x^λ with $\lambda > 0$ (real). In Sect. 2.1, we show that the new eigenvalues are determined by a one-dimensional eigenvalue problem in the limit of the exterior fluid and boundary surface having the same temperature ($\mathrm{G} \ll 1$). If the externally imposed pressure gradient is sufficiently large and favourable ($\beta > \beta_c$) then λ becomes negative and the modes decay downstream. In Sects. 2.2.1 and 2.2.2, we show that values for β_c can be obtained asymptotically in the limits of large/small Prandtl number.

Clearly, the constraint of a surface temperature variation of the form $x^{(3n-1)/2}$ is restrictive, so we will place most attention on the case $H_w = 0$ (hence $H \equiv 0$). In this scenario, the bulk surface and far-field fluid are at the same temperature but we can still allow for spatially localised temperature deviations of size ΔT^*. In this approach, the Grashof parameter G becomes a measure of the amplitude of this localised thermal forcing. In Sect. 3, we march the nonlinear and non-self-similar system (6) in x, solving in the Y, Z-plane (equivalently the η, ζ-plane) for a localised 'hot spot' forcing on the boundary. We show that the growing eigenmodes are recovered downstream in the linear regime, developing into fully nonlinear (non-self-similar) streaks at larger forcing. The nonlinear downstream development provides a structure upon which inviscid secondary instabilities can grow. In Sect. 4, we briefly explore the stability to Rayleigh instabilities in the cross-section plane of a fixed downstream position.

2 Linear algebraic eigenmodes in forced convection

We seek spatially developing steady eigenmodes analogous to those found for the isothermal Blasius ($n = 0$) boundary layer by Hewitt and Duck [12] but extended to include buoyancy coupling with the energy equation and an external pressure gradient ($n > 0$, as formulated in [17]). These exist in the form

$$\hat{U} = x^n U(x,\eta,\zeta), \quad (\hat{V},\hat{W}) = \left(\frac{n+1}{2}\right)^{1/2} x^{\frac{n-1}{2}}\,(V(x,\eta,\zeta), W(x,\eta,\zeta)), \quad \hat{\vartheta} = x^{\frac{3(n-1)}{2}}\vartheta(x,\eta,\zeta), \tag{9a}$$

with

$$U = U_B(\eta) + \epsilon x^\lambda \tilde{U}(\eta,\zeta) + \cdots, \quad V = V_B(\eta) + \epsilon x^\lambda \tilde{V}(\eta,\zeta) + \cdots, \tag{9b}$$

$$W = \epsilon x^\lambda \tilde{W}(\eta,\zeta) + \cdots, \quad \vartheta = \vartheta_B(\eta) + \epsilon x^\lambda \tilde{\vartheta}(\eta,\zeta) + \cdots, \tag{9c}$$

where the base flow is a (two-dimensional) Falkner–Skan boundary layer with $U_B(\eta) \equiv F'(\eta)$, $V_B(\eta) \equiv [(1-n)/(1+n)]\eta F'(\eta) - F(\eta)$ and $\vartheta_B(\eta) \equiv H(\eta)$ as described by (8). Here $\epsilon \ll 1$ for linear disturbances

and the spanwise coordinate ζ is scaled with the local boundary-layer thickness such that both coordinates in the cross section are

$$(\eta, \zeta) = \left(\frac{n+1}{2}\right)^{\frac{1}{2}} x^{\frac{n-1}{2}} (Y, Z). \tag{9d}$$

The η coordinate simply matches the Falkner–Skan similarity form (8), so as the solution develops downstream the spanwise length scale remains comparable to the local boundary-layer thickness. The downstream dependence of the $O(\epsilon)$ perturbation is entirely captured by the algebraic dependence of x^{λ} and (9d), so these modes apply at all downstream positions despite the non-parallel nature of the problem.

The dominant modes are such that $\lambda \in \mathfrak{Re}$ and therefore when $\lambda > 0$ these three-dimensional eigenmodes grow algebraically downstream relative to the two-dimensional base flow velocity field. For isothermal ($\tilde{\vartheta} \equiv 0$) disturbances applied to a Blasius boundary layer ($n = 0$) it is known that such modes exist but that they *decay* ($\lambda < 0$) away from the leading edge [12].

Substitution of (9) into (6) gives a bi-global eigenvalue problem for the spatial growth 'rate' λ as a function of the Prandtl number (Pr) and pressure gradient parameter (β or equivalently n). To avoid explicit treatment of the pressure in (6) it is convenient to cross-differentiate to eliminate $\hat{P}$ in favour of a vorticity component ($\tilde{\Theta}$) and then use a substitution

$$\tilde{V} = \frac{1-n}{1+n}\eta\tilde{U}(\eta,\zeta) - \tilde{\Phi}(\eta,\zeta), \quad \tilde{W} = \frac{1-n}{1+n}\zeta\tilde{U}(\eta,\zeta) - \tilde{\Psi}(\eta,\zeta), \tag{10a}$$

which mirrors that appear in the standard Falkner–Skan solution (8). The resulting bi-global eigenvalue problem is, on replacing $n = \beta/(2-\beta)$:

$$0 = (2-\beta)(\lambda+1)\tilde{U} - \tilde{\Phi}_\eta - \tilde{\Psi}_\zeta, \tag{11a}$$

$$\tilde{\Theta} = \tilde{\Psi}_\eta - \tilde{\Phi}_\zeta, \tag{11b}$$

$$\bar{\nabla}^2\tilde{U} = 2\beta F'\tilde{U} + (2-\beta)\lambda F'\tilde{U} - F\tilde{U}_\eta - \zeta(1-\beta)F'\tilde{U}_\zeta - F''\tilde{\Phi}, \tag{11c}$$

$$\begin{aligned}\bar{\nabla}^2\tilde{\Theta} = {} & 2(1-\beta)[\zeta F'\tilde{U}_\eta + \zeta F''\tilde{U} - \eta F'\tilde{U}_\zeta] - F\tilde{\Theta}_\eta - \zeta(1-\beta)F'''\tilde{\Phi} \\ & - \zeta(1-\beta)F'\tilde{\Theta}_\zeta - (1-\beta)F''\tilde{\Psi} - (2-\beta)[F'\tilde{\Theta} + \zeta(1-\beta)F''\tilde{U}] \\ & + (2-\beta)\lambda[F''\tilde{\Psi} + F'\tilde{\Theta} - \zeta(1-\beta)F''\tilde{U}] - (2-\beta)^{\frac{3}{2}}\mathrm{G}\tilde{\vartheta}_\zeta,\end{aligned} \tag{11d}$$

$$\frac{1}{\mathrm{Pr}}\bar{\nabla}^2\tilde{\vartheta} = [(2-\beta)\lambda - 3(1-\beta)]F'\tilde{\vartheta} - F\tilde{\vartheta}_\eta - \zeta(1-\beta)F'\tilde{\vartheta}_\zeta - H'\tilde{\Phi} - 3(1-\beta)\tilde{U}H, \tag{11e}$$

where $\bar{\nabla}^2$ is the two-dimensional Laplacian in the (η, ζ) plane. The velocity-field conditions on the plate ($\eta = 0$) are no-slip and impermeability, whilst the disturbance field decays to zero for sufficiently large values of η or ζ. The temperature disturbance remains zero both at the boundary and far field. This bi-global eigenvalue spectrum for λ will obviously include the isothermal Hewitt and Duck [12] *decaying* ($\lambda < 0$) eigenmodes for $\mathrm{G} \ll 1$ (with $\tilde{\vartheta} = 0$), but is here also augmented by new thermal modes ($\tilde{\vartheta} \neq 0$) which are the focus of our current discussion.

In the limit of a small Grashof parameter $\mathrm{G} \ll 1$ the energy equation decouples in (11); this version of the eigenproblem is also recovered if the bulk surface temperature is the same as the far-field fluid, that is $H_w = 0$ ($H \equiv 0$).

The problem is solved with a second-order finite-difference scheme that spans $N_\eta \times N_\zeta$ nodes, resulting in a generalised eigenvalue problem of size $5N_\eta N_\zeta \times 5N_\eta N_\zeta$. A non-uniform mesh is applied to improve resolution near to the origin and `SLEPc` (Hernandez et al. [18]) is employed to make use of (iterative) sparse matrix methods. Solutions presented below are independent of the mesh resolution and domain truncation, but typical resolutions are $N_\eta = N_\zeta = 600$ over a truncated domain size of $(\eta, \zeta) \in [0, 40] \times [0, 40]$.

The eigenvalue spectrum varies with the Prandtl number Pr, pressure gradient β and Grashof parameter G. As a representative example, we present eigenvalues determined from the bi-global eigenvalue problem for Prandtl

Table 1 The first six eigenvalues λ determined from the bi-global computation of (11) with varying Grashof number G, $\beta = 0$ (a Blasius base flow) and Prandtl number Pr = 0.71

G	λ_1	λ_2	λ_3	λ_4	λ_5	λ_6
0	0.203	− 0.723	− 0.777	− 0.797	− 1.242	− 1.500
10^{-2}	0.203	− 0.723	− 0.777	− 0.797	− 1.242	− 1.500
1	0.203	− 0.723	− 0.778	− 0.795	− 1.242	− 1.442
2	0.203	− 0.722	− 0.778	− 0.794	− 1.242	− 1.389

The least damped eigenvalue λ_1 is positive, and so the eigenmode has an algebraic spatial growth downstream from the leading edge. The modes presented by Hewitt and Duck [12] now couple with the temperature field, but for $G \ll 1$ remain isothermal. The new thermal modes presented here in this limit are λ_1, λ_2 and λ_4. Here, the domain is truncated at $\eta = \zeta = 60$

number Pr = 0.71 (air at room temperature), no pressure gradient $\beta = 0$ and varying G in Table 1. The decaying $\tilde{\vartheta} \equiv 0$ modes of Hewitt and Duck [12] are present in the bi-global eigenvalue calculations with $G \ll 1$.

The least damped eigenvalue $\lambda_1 = 0.203$ presented in Table 1 for $G \ll 1$ represents an algebraically growing thermal mode embedded in a Blasius base flow. The velocity field grows downstream with spatial growth $x^{0.203}$ (for the streamwise velocity), whilst the temperature field decays with $x^{-1.297}$. The first few least damped eigenmodes are only weakly varying with G (which motivates the analysis of Sect. 2.1 below) but the spatial growth of the first mode increases at sufficiently large values of G.

The first three $G = 1$ thermal eigenmodes associated with λ_1, λ_2 and λ_4 of Table 1 are shown in Fig. 1. The dominant mode is shown in the top sub-figure (a). The eigenmodes are localised, and a streamwise-aligned streak is exhibited with associated in-plane rolls. The modes are assumed to be symmetric about the $\zeta = 0$ midplane for $\tilde{U}$, $\tilde{V}$, $\tilde{\vartheta}$ and antisymmetric for $\tilde{W}$; the eigenmodes are therefore only shown for $\zeta > 0$.

At finite values of the Grashof parameter G, we solve the bi-global eigenvalue problem as described above. However, in the limit of $G \ll 1$ it is possible to make some progress with an alternative description that provides some insight into the new (thermal) eigenvalue distribution in Table 1.

2.1 Classification of the eigenvalues

In the limit of small Grashof parameter, or equivalently under the assumption that the exterior fluid and boundary surface have the same temperature ($H_w = 0$), we note that the energy equation (11e) becomes decoupled from the velocity perturbations and may be solved independently. The isothermal Hewitt and Duck [12] modes are recovered in this limit, and so we may restrict our attention to the new eigenvalues associated with thermal effects, the first six of which are given in Table 2.

It can be seen from Table 2 that some of the $G \ll 1$ thermal eigenvalues are related by an integer difference, namely

$$\lambda_1 = \lambda_4 + 1 = \lambda_{10} + 2, \quad \lambda_2 = \lambda_9 + 1. \tag{12}$$

To explain this behaviour and provide an alternative to the bi-global computational method in this limiting case, we expand for $G \ll 1$

$$\tilde{\vartheta} = \tilde{\vartheta}_0 + O(G), \quad (\tilde{U}, \tilde{\Phi}, \tilde{\Psi}, \tilde{\Theta}) = \mathrm{G}(\tilde{U}_0, \tilde{\Phi}_0, \tilde{\Psi}_0, \tilde{\Theta}_0) + O(G^2), \quad \lambda = \lambda^{(0)} + O(G), \tag{13}$$

and consider the spanwise Fourier transform of (11e) via

$$L(\eta, k) = \int_{-\infty}^{\infty} \tilde{\vartheta}_0(\eta, \zeta)\, \exp(-\mathrm{i}k\zeta)\mathrm{d}\zeta. \tag{14}$$

The transformed temperature component of the bi-global eigenvalue problem (11e) results in (on dropping the superscript zero on the leading-order eigenvalue)

$$\frac{1}{\mathrm{Pr}}(L_{\eta\eta} - k^2 L) = [(2-\beta)\lambda - 2(1-\beta)]F'L - FL_\eta + (1-\beta)F'kL_k, \tag{15}$$

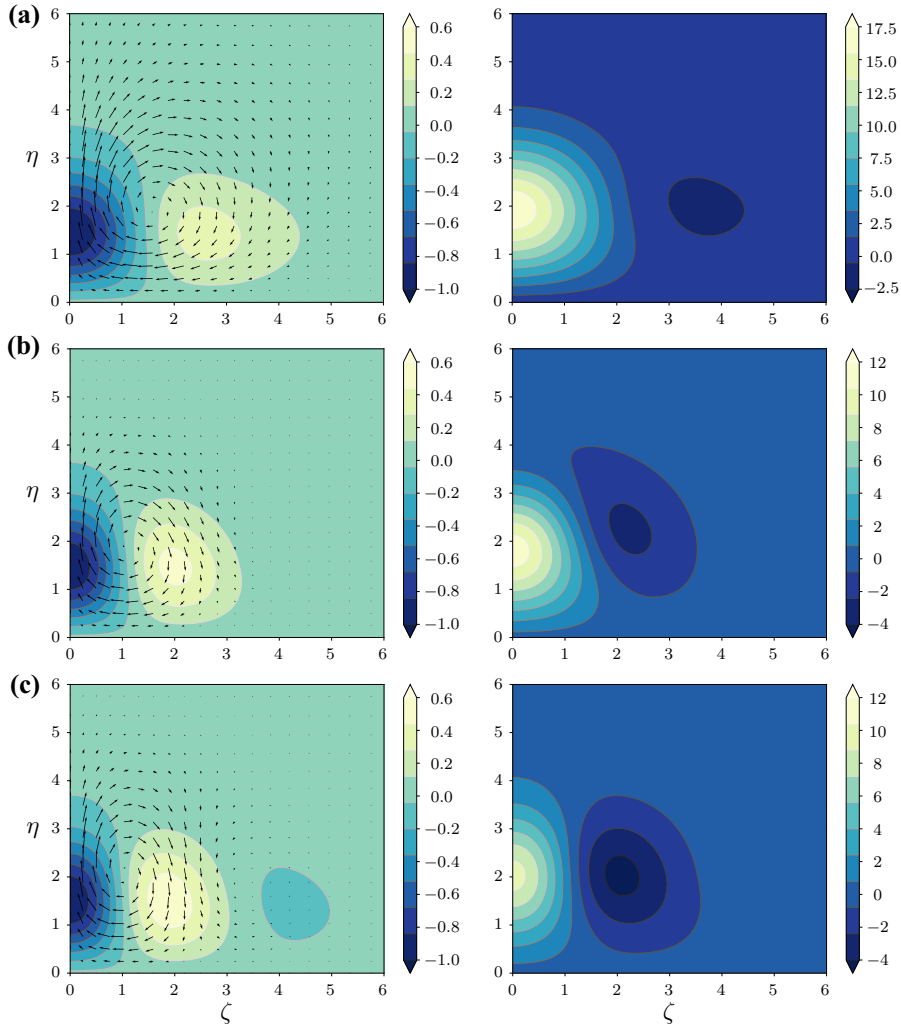

Fig. 1 Temperature and velocity fields for **a** the growing $\lambda = 0.203$ mode, and the decaying **b** $\lambda = -0.723$, **c** $\lambda = -0.797$ modes listed in Table 1 for $G = 1$. The Prandtl number is taken to be Pr$= 0.71$ and no pressure gradient is applied $\beta = 0$ (Blasius flow). On the left, the streamwise velocity of the eigenmode $\tilde{U}$ is overlaid by the $(\tilde{V}, \tilde{W})$ roll vector field. On the right, the corresponding scaled temperature $\tilde{\vartheta}$ distribution is shown. Each mode is normalised such that $\tilde{U}$ has a minimum of -1. Only the half-plane $\zeta > 0$ is shown with $\zeta < 0$ obtained by reflection

Table 2 The first six (thermal mode) eigenvalues λ determined from the bi-global computation of (11) in the limit $G \ll 1$, with $\beta = 0$ and Pr $= 0.71$. The isothermal eigenvalues of Hewitt and Duck [12] are excluded here but their values are included in Table 1 with $G \ll 1$ for λ_3, λ_5 and λ_6, whilst $\lambda_8 = -1.693$

λ_1	λ_2	λ_4	λ_7	λ_9	λ_{10}
0.203	− 0.723	− 0.797	− 1.668	− 1.723	− 1.797

for which we have written the base flow quantities in terms of the Falkner–Skan profile $F(\eta)$ defined by (8), and we have used the fact that $\mathcal{F}\{-\zeta\tilde{\vartheta}_{0\zeta}\} = L + kL_k$.

The eigenfunctions of Fig. 1 are symmetric about $\zeta = 0$ (for the temperature field), hence in the limit $k \ll 1$ we introduce the small wavenumber expansion

Table 3 The first five greatest eigenvalues $\Lambda = \Lambda_i$, with $i = 1, 2, ..., 5$, as determined from the one-dimensional eigenvalue problem (17) with the substitution (18) for a Blasius base flow ($\beta = 0$) with Prandtl number Pr = 0.71

Λ_1	Λ_2	Λ_3	Λ_4	Λ_5
0.203	− 0.723	− 1.668	− 2.622	− 3.583

Table 4 The one-dimensional eigenvalue problem for Λ predicts the G $\ll 1$ thermal bi-global eigenvalue spectrum for λ, by varying the integer m in relation (18). These results are generated for a Blasius base flow $\beta = 0$ and Prandtl number Pr = 0.71. The values λ_i are as presented in Table 2

m	$\Lambda_1 - m$	$\Lambda_2 - m$	$\Lambda_3 - m$	$\Lambda_4 - m$	$\Lambda_5 - m$
0	0.203 ($= \lambda_1$)	− 0.723 ($= \lambda_2$)	− 1.668 ($= \lambda_7$)	− 2.622	− 3.583
1	− 0.797 ($= \lambda_4$)	− 1.723 ($= \lambda_9$)	− 2.668	− 3.622	− 4.583
2	− 1.797 ($= \lambda_{10}$)	− 2.723	− 3.668	− 4.622	− 5.583
3	− 2.797	− 3.723	− 4.668	− 5.622	− 6.583

$$L(\eta, k) = k^{2m} L_m(\eta) + \cdots, \tag{16}$$

for some $m \in \mathbb{N}_0$. The leading-order term for the disturbance temperature field then satisfies the ordinary-differential eigenvalue problem:

$$\frac{1}{\mathrm{Pr}} L_m'' = [(2-\beta)\lambda + (2m-2)(1-\beta)] F' L_m - F L_m', \tag{17}$$

subject to $L_m(0) = L_m(\infty) = 0$. Having established the leading-order term via this approach, it is then possible to march (15) (in wavenumber space) from $k = 0$ to large-k provided that $(1-\beta)F'(\eta) > 0$ for all η, which certainly holds for $0 \leq \beta < 1$. The computational scheme begins with the leading-order term $L_m(\eta)$ at $k = 0$ and solves for $L(\eta, k)$ at successive k stations. The full solution to $L(\eta, k)$ then yields $\tilde{\vartheta}_0$ via the inverse Fourier transform. Taking this approach avoids the bi-global method (in this G $\ll 1$ limit), but the associated velocity field must still be determined globally by solving the forced elliptic problem that arises from (11a)–(11d). However, the form of (17) provides an explanation of the integer differences noted above in (12).

For the one-dimensional eigenvalue equation (17), the explicit dependence of the integer m can be removed by introducing a new eigenvalue Λ, where

$$\Lambda = \lambda + \frac{2m(1-\beta)}{2-\beta}; \tag{18}$$

note that the dependence on β will always persist through the baseflow terms $F(\eta)$ and $F'(\eta)$ via the Falkner–Skan equation (8). In Table 3, we show the first five eigenvalues for Λ when evaluated for $\beta = 0$ (Blasius) with Pr = 0.71.

The G $\ll 1$ thermal eigenvalues λ obtained from the full bi-global eigenvalue problem (Table 2) are related to the one-dimensional eigenvalues Λ (Table 3) via the integer m, through relation (18). To demonstrate this for a Blasius base flow (for which (18) reduces to $\lambda = \Lambda - m$), we show Table 4 by subtracting $m = 0, 1, 2, \cdots$.

The bi-global G $\ll 1$ eigenmodes for λ_1 and λ_4 (for example, as shown in Fig. 1) when Fourier transformed in ζ and evaluated for $k \ll 1$ should have the same η dependence in the leading-order term of (16); this is confirmed in Fig. 2.

2.2 The pressure gradient and Prandtl number (β-Pr) parameter space

We now continue with the formulation (17) to determine the dependence of the spatial growth/decay exponent λ on the pressure gradient β and Prandtl number Pr.

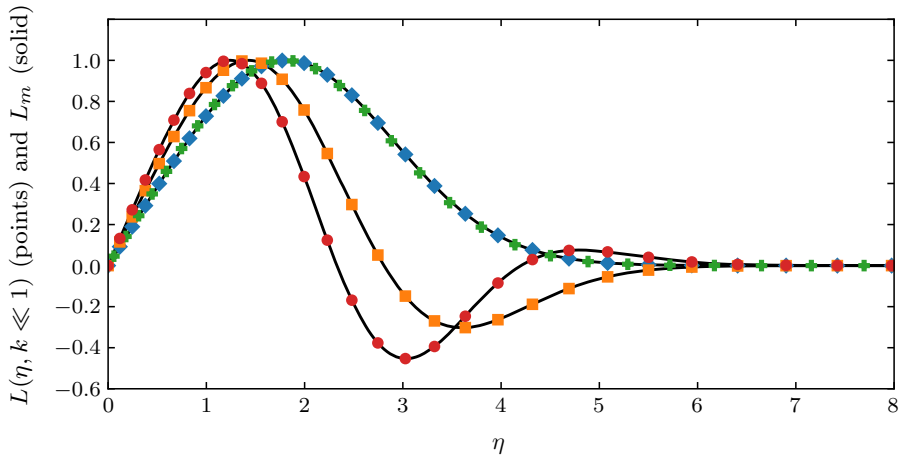

Fig. 2 The Fourier transform of the temperature field (14), as obtained from the bi-global G $\ll$ 1 eigenproblem computation, evaluated for $k \ll 1$ (points) compared with the one-dimensional eigenvalue problem (17) (solid lines). The Fourier transform of the bi-global eigenfunctions correspond to λ_1 (diamonds), λ_2 (squares), λ_4 (plus signs) and λ_7 (circles), the eigenvalues for which are presented in Table 2. Here Pr $= 0.71$ and $\beta = 0$, and solutions have been normalised to have a maximum of unity

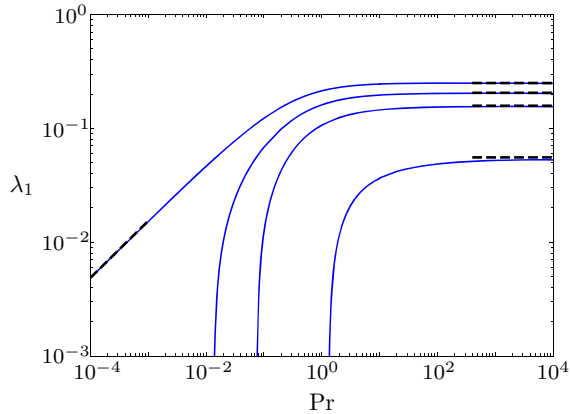

Fig. 3 The dominant algebraic growth rate λ_1 determined for a Falkner–Skan boundary layer with $\beta = 0, 0.05, 0.1, 0.2$. The growth rate diminishes with increasing β. Also plotted are the asymptotic predictions of $\lambda_1 = \frac{1}{4}, \frac{8}{39}, \frac{3}{19}, \frac{1}{18}$ for Pr $\gg 1$ and $\lambda_1 = 0.4854\text{Pr}^{\frac{1}{2}}$ for Pr $\ll 1$ (dashed)

Figure 3 presents the dominant (growing) eigenvalue λ_1 as a function of Pr for $\beta = 0, 0.05, 0.1, 0.2$. The eigenvalue for $\beta = 0$ remains positive for all Prandtl numbers, corresponding to an algebraically growing thermal eigenmode. Increasing the Prandtl number leads to an increase of the downstream growth λ_1 up to a limiting value of $\frac{1}{4}$ for $\beta = 0$.

As expected, the addition of a favourable pressure gradient β diminishes the eigenvalue λ_1 for any given Prandtl number. Figure 4 shows the critical neutral ($\lambda_1 = 0$) boundary in the β-Pr parameter space. For $\beta > \frac{1}{4}$ the mode is stabilised at all values of Pr. We shall discuss the large and small Prandtl asymptotes in Sects. 2.2.1 and 2.2.2. We will also show that the asymptotes for the dominant eigenvalues of Fig. 3 follow from the same analysis.

2.2.1 The Pr $\ll 1$ *asymptote of the neutral curve*

We can describe the low Pr limit of (17) with $\lambda = 0$ (to capture the neutral case) and $m = 0$ (for the dominant mode), which reduces to

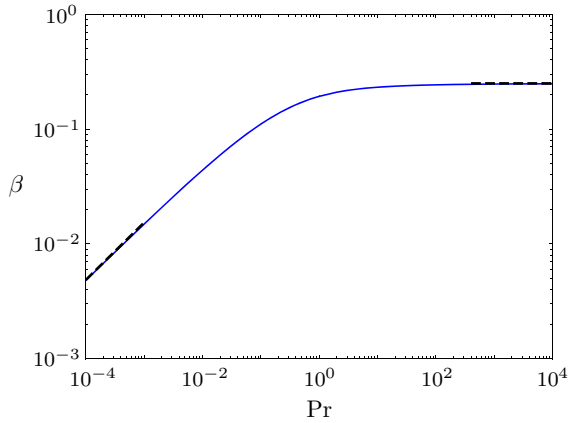

Fig. 4 The neutral curve for which the dominant eigenvalue is $\lambda_1 = 0$. Above the neutral curve, the dominant thermal eigenmode decays, whilst below the neutral curve it grows. Also plotted are the asymptotic predictions of $\beta = \frac{1}{4}$ for $\mathrm{Pr} \gg 1$ and $\beta = 0.4854\mathrm{Pr}^{\frac{1}{2}}$ for $\mathrm{Pr} \ll 1$ (dashed)

$$\frac{1}{\mathrm{Pr}} L_0''(\eta) = 2(\beta - 1)F'(\eta;\beta)L_0(\eta) - F(\eta;\beta)L_0'(\eta), \quad L_0(0) = L_0(\infty) = 0, \tag{19}$$

for which $\beta \equiv \beta(\mathrm{Pr})$ and F satisfies the Falkner–Skan equation (8). This represents an eigenvalue problem in β for varying Prandtl number (or vice versa).

For small Prandtl number ($\mathrm{Pr} \ll 1$), the thermal boundary layer thickens, whilst the momentum boundary layer of the underlying Falkner–Skan base flow remains on the $\eta = O(1)$ scale. We therefore seek an expansion in an outer region defined by $\hat{\eta} = \eta\,\mathrm{Pr}^{\frac{1}{2}} = O(1)$ of the form

$$L_0(\hat{\eta}) = L_{00}(\hat{\eta}) + \mathrm{Pr}^{\frac{1}{2}} L_{01}(\hat{\eta}) + \cdots, \tag{20a}$$

$$F(\hat{\eta}) = \mathrm{Pr}^{-\frac{1}{2}}\hat{\eta} + \delta(\beta = 0) + \cdots, \tag{20b}$$

$$\beta = \beta_1 \mathrm{Pr}^{\frac{1}{2}} + \cdots, \tag{20c}$$

where $\delta(\beta = 0) \approx -1.217$ is the displacement associated with the Blasius solution.

Leading-order $L_{00}(\hat{\eta})$ is governed by

$$L_{00}'' = -2L_{00} - \hat{\eta}L_{00}', \quad L_{00}(0) = L_{00}(\infty) = 0, \tag{21a}$$

with solution $L_{00} = C\hat{\eta}\exp(-\hat{\eta}^2/2)$, for constant C.

In the inner layer for which $\eta = O(1)$, the diffusion term dominates the temperature field, and we recover a linear profile for $L_0(\eta)$, which matches to the outer solution.

The constant β_1 in (20) is only determined at higher order via

$$L_{01}''(\hat{\eta}) + \hat{\eta}L_{01}'(\hat{\eta}) + 2L_{01}(\hat{\eta}) = 2\beta_1 L_{00}(\hat{\eta}) - \delta(\beta = 0)L_{00}'(\hat{\eta}), \tag{22}$$

or in terms of the analytic solution for $L_{00}(\hat{\eta})$,

$$L_{01}''(\hat{\eta}) + \hat{\eta}L_{01}'(\hat{\eta}) + 2L_{01}(\hat{\eta}) = C\mathrm{e}^{-\frac{\hat{\eta}^2}{2}}[2\beta_1\hat{\eta} - \delta(\beta = 0)(1 - \hat{\eta}^2)]. \tag{23}$$

This can be written as a Sturm–Liouville problem with homogeneous boundary conditions,

$$L_{00}(\hat{\eta})\frac{\mathrm{d}}{\mathrm{d}\hat{\eta}}\left(\mathrm{e}^{\frac{\hat{\eta}^2}{2}} L_{01}'(\hat{\eta})\right) + 2\mathrm{e}^{\frac{\hat{\eta}^2}{2}} L_{00}(\hat{\eta})L_{01}(\hat{\eta}) = CL_{00}(\hat{\eta})[2\beta_1\hat{\eta} - \delta(\beta = 0)(1 - \hat{\eta}^2)]. \tag{24}$$

Noting that this problem is self adjoint, and that

$$\frac{\mathrm{d}}{\mathrm{d}\hat{\eta}}\Big(\mathrm{e}^{\frac{\hat{\eta}^2}{2}} L_{00}'(\hat{\eta})\Big) + 2\hat{\eta}\mathrm{e}^{\frac{\hat{\eta}^2}{2}} L_{00}(\hat{\eta}) = 0, \tag{25}$$

we therefore have the solvability condition

$$\beta_1 = \frac{\delta(\beta=0)\int_0^\infty (1-\hat{\eta}^2)\hat{\eta}\mathrm{e}^{-\frac{\hat{\eta}^2}{2}}\mathrm{d}\hat{\eta}}{2\int_0^\infty \hat{\eta}^2\mathrm{e}^{-\frac{\hat{\eta}^2}{2}}\mathrm{d}\hat{\eta}} = -\frac{\delta(\beta=0)}{\sqrt{2\pi}}. \tag{26}$$

The displacement in the far field for the Blasius solution is $\delta(\beta=0)\approx -1.217$, which results in the asymptotic prediction $\beta_1 \approx 0.4854$. This prediction of $\beta \approx 0.4854\,\mathrm{Pr}^{\frac{1}{2}}$ is plotted for $\mathrm{Pr}\ll 1$ on the neutral curve presented in Fig. 4.

The above analysis for the neutral curve asymptote with $\mathrm{Pr}\ll 1$ also gives the asymptotic behaviour of the algebraic growth rate λ_1 in this same limit when $\beta=0$; as shown in Fig. 3. This is because the eigenvalue problem for λ_1 with $\beta=0$ is precisely the same problem (19) but with $2(\beta-1)$ replaced by $2(\lambda_1-1)$.

2.2.2 *The* $\mathrm{Pr}\gg 1$ *asymptote of the neutral curve*

In the large Prandtl $\mathrm{Pr}\gg 1$ limit, the thermal boundary layer becomes thinner, whilst again the base flow remains on the $\eta = O(1)$ scale. In the inner layer, for small η the Falkner–Skan solution is to the leading order approximated by $F=\tau\eta^2/2$, where τ is related to the wall shear $\tau = F''(0;\beta=\beta_c)$ and β_c is a critical pressure gradient to be determined as part of the solution below.

To capture this inner layer we introduce $\bar{\eta}=\eta\,\mathrm{Pr}^{\frac{1}{3}}$, and look for expansions in the form

$$L_0 = \bar{L}_{00}(\bar{\eta})+\cdots, \quad F = \mathrm{Pr}^{-\frac{2}{3}}\frac{\tau\bar{\eta}^2}{2}+\cdots, \tag{27}$$

leading to

$$\bar{L}_{00}''(\bar{\eta}) = 2(\beta-1)\tau\bar{\eta}\bar{L}_{00}(\bar{\eta}) - \frac{\tau\bar{\eta}^2}{2}\bar{L}_{00}'(\bar{\eta}). \tag{28}$$

Through a change of coordinates

$$\xi = -\frac{\tau\bar{\eta}^3}{6}, \tag{29}$$

with $\bar{L}_{00}(\eta)=\hat{L}_{00}(\xi)$ the inner layer equation (28) is reduced to

$$\xi\hat{L}_{00}''(\xi) + \Big(\frac{2}{3}-\xi\Big)\hat{L}_{00}'(\xi) - \frac{4}{3}(1-\beta)\hat{L}_{00}(\xi) = 0, \tag{30}$$

and thus permits confluent hypergeometric solutions

$$\bar{L}_{00}(\bar{\eta}) = C_1\,{}_1F_1\Big(-\frac{4}{3}(\beta-1);\frac{2}{3};-\frac{\tau\bar{\eta}^3}{6}\Big) + C_2\bar{\eta}\,{}_1F_1\Big(\frac{5}{3}-\frac{4}{3}\beta;\frac{4}{3};-\frac{\tau\bar{\eta}^3}{6}\Big), \tag{31}$$

for constants C_1 and C_2. On the boundary we have $\hat{L}_{00}(0)=0$, and so $C_1=0$. In the limit $\bar{\eta}\to\infty$, the confluent hypergeometric function takes the asymptotic form

$$\bar{L}_{00}(\bar{\eta}) \sim C_2\bar{\eta}\Big(\frac{D_1\bar{\eta}^{1-4\beta}\mathrm{e}^{-\frac{\tau\bar{\eta}^3}{6}}}{\Gamma\big(\frac{5}{3}-\frac{4\beta}{3}\big)} + \frac{D_2\bar{\eta}^{4\beta-5}}{\Gamma\big(\frac{4\beta}{3}-\frac{1}{3}\big)}\Big), \tag{32}$$

for known non-zero constants D_1 and D_2, see Abramowitz and Stegun [19]. For non-algebraic decay into the far field we require that $\Gamma(\frac{4\beta}{3}-\frac{1}{3})$ is singular. As the Gamma function has simple poles at arguments of $l=0,-1,-2,\cdots$, exponential decay of the thermal mode only occurs for $\beta=(1+3l)/4$, and therefore for $\beta>0$, a solution only exists for a single value of the pressure gradient (Hartree) parameter of $\beta=\frac{1}{4}$.

The $\mathrm{Pr} \gg 1$ asymptotic behaviour of the dominant algebraic growth rate for varying β (Fig. 3) can be similarly determined by noting the eigenvalue problem for λ_1 is the same problem (28) but now with $2(\beta - 1)$ replaced by $[(2-\beta)\lambda_1 - 2(1-\beta)]$. The same analysis therefore leads to the $\mathrm{Pr} \gg 1$ behaviour

$$\lambda_1 \to \frac{1}{2}\left[\frac{1-4\beta}{2-\beta}\right], \tag{33}$$

which for $\beta = 0, 0.05, 0.1, 0.2$, evaluates to $\lambda_1 \to \frac{1}{4}, \frac{8}{39}, \frac{3}{19}, \frac{1}{18}$, respectively. These asymptotes are included in Fig. 3.

3 Nonlinear (non-self-similar) downstream development

Having established the existence of growing linear eigenmodes, we now tackle the fully nonlinear and non-self-similar problem defined by (6). A reformulation of (6) in terms of a three-dimensional perturbation to a two-dimensional base flow of (8) is given in Appendix A and it is this form of the problem that we solve numerically in this section.

We restrict attention to the case of only a localised temperature difference between the surface and exterior fluid, this corresponds to taking $H_w = 0$ in (8) such that $H \equiv 0$. To initiate a steady disturbance an ad hoc smooth localised surface temperature is forced in the form

$$\hat{\vartheta}(x, \eta = 0, \zeta) = \mathrm{e}^{-\gamma(x-x_0)^2}\mathrm{e}^{-c\zeta^2}. \tag{34}$$

This forcing is centred on x_0, and its streamwise and spanwise extents are set by γ and c. Herein, we present solutions for $\gamma = 10$ and $c = 1$ as representative values. Even assuming $H \equiv 0$ we retain the Grashof parameter G by defining the temperature measure ΔT^* as the peak difference associated with the hot spot defined by (34); hence in this case the amplitude of the spatially localised forcing becomes parameterised by the Grashof parameter G.

We employ parabolic marching in the streamwise x coordinate, using a second-order Crank–Nicolson finite-difference scheme for successive x locations, solving in the cross-sectional Y, Z plane. Rather than Y and Z we use the η and ζ coordinates for computational convenience, but the scheme does *not* assume any self-similarity in the flow. In the cross-sectional plane the system is discretised over a non-uniform mesh of size $N_\eta \times N_\zeta$. We start the marching procedure with trivial initial conditions at $x = 0$, at which point the forcing (34) is exponentially small and negligible (being much less than the convergence tolerance employed in the numerical scheme). At each x step thereafter and with each Newton iteration, we solve a sparse linear system of size $5N_\eta N_\zeta \times 5N_\eta N_\zeta$. The linear solve phase is enabled by use of a sparse parallel formulation in the C++ library PETSc (Balay et al., [20]).

To assess the downstream development of the disturbances, we employ the global measure suggested by Andersson et al. [21],

$$\mathcal{A}(x) = \frac{1}{2}\left[\max_{Y,Z}(U - U_B) - \min_{Y,Z}(U - U_B)\right], \tag{35}$$

for which $U_B = F'(\eta)$ is the Falkner–Skan solution and U is as defined by (9a). The measure $\mathcal{A}$ indicates the amount that the disturbance deviates from the underlying Falkner–Skan boundary layer.

We exhibit the measure $\mathcal{A}$ in Fig. 5 for streaks determined using a Grashof parameter of $\mathrm{G} = \frac{1}{2}, 1, 2, 4, 8, 16$ with $\mathrm{Pr} = 0.71$. The streaks are embedded in a Blasius boundary layer ($\beta = 0$), and the plate heating (34) is centred on $x_0 = 10$. The $x^{0.203}$ algebraic growth of the dominant linearised eigenmode given in Table 1 is also plotted as a line segment. The streaks exhibit this algebraic growth for small Grashof parameter (i.e. low forcing amplitude). Cross sections of the $G = 16$ streak depicted in Fig. 5 are shown in Fig. 6 at $x = 20$ and $x = 250$.

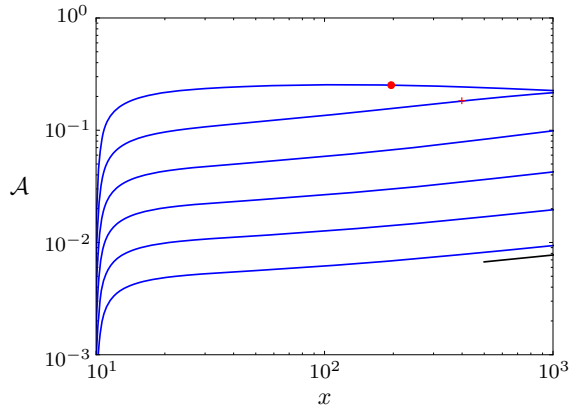

Fig. 5 The magnitude of streaks generated by a localised heated region (34) located at $x = x_0 = 10$ for varying amplitudes $\mathrm{G} = \frac{1}{2}, 1, 2, 4, 8, 16$ and measured by $\mathcal{A}$ (35). Here $x_0 = 10$, $\mathrm{Pr} = 0.71$, $\beta = 0$ (a Blasius layer) and $H \equiv 0$. Lower amplitude streaks exhibit the predicted linear $x^{0.203}$ algebraic growth, shown by the (black) line segment. Unstable inviscid Rayleigh modes develop for the $\mathrm{G} = 8$ and $\mathrm{G} = 16$ streaks. The $\mathrm{G} = 16$ streak is unstable to a sinuous Rayleigh mode at the heated region. Points show the first appearance of further Rayleigh instabilities downstream, with sinuous modes (plus-sign) at lower amplitudes than varicose modes (circle)

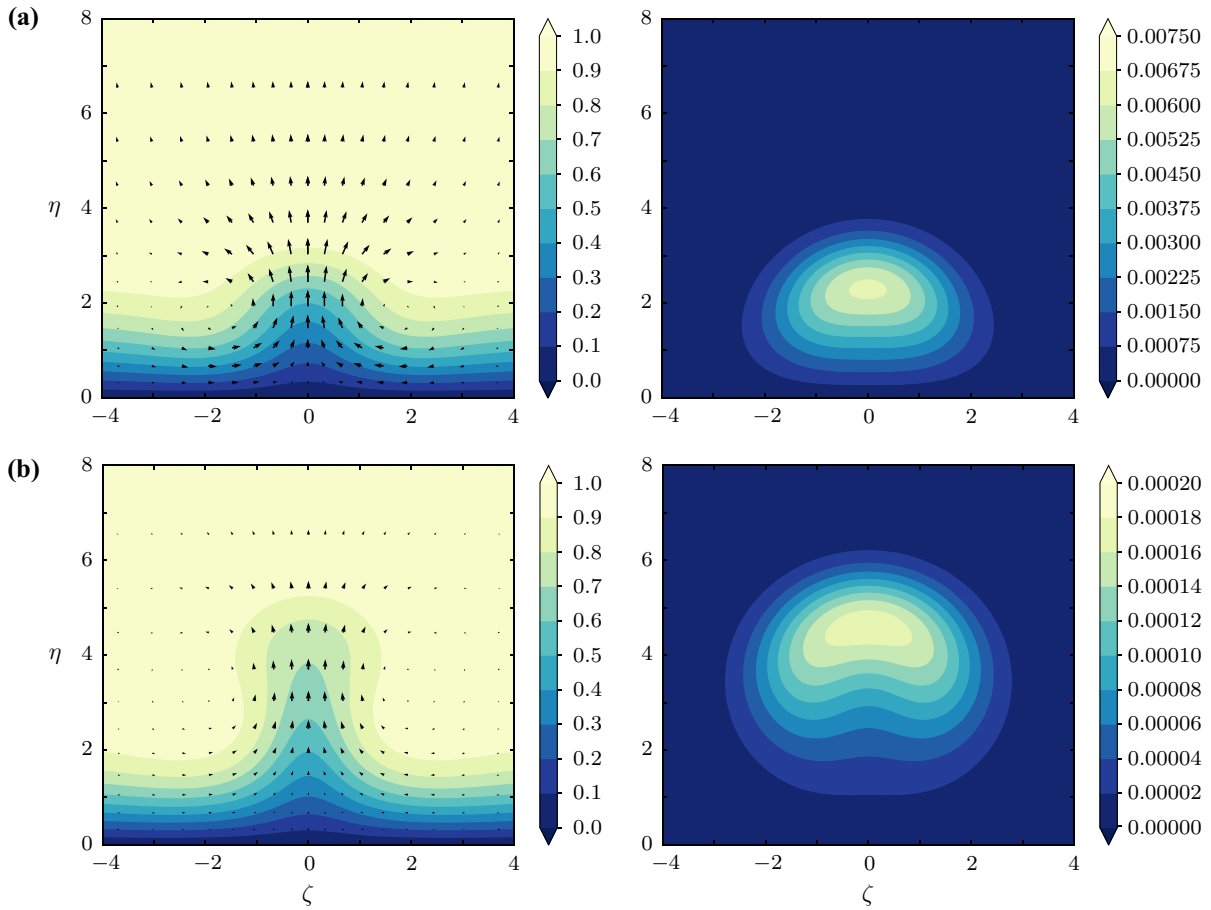

Fig. 6 The nonlinear streak response at **a** $x = 20$ and **b** $x = 250$ to wall heating (34) localised to $x = x_0 = 10$. The streak is embedded in a Blasius boundary layer ($\beta = 0$) with Grashof parameter $\mathrm{G} = 16$ and Prandtl number $\mathrm{Pr} = 0.71$. Depicted are the streamwise velocity $\hat{U}$ with the $(\hat{V}, \hat{W})$ roll field overlaid (left), and the temperature $\hat{\vartheta}$ (right)

4 Inviscid stability of the nonlinear streaks

In the developing streak there is a downstream velocity $\hat{U}(x, Y, Z)$ as defined in (5). To assess the inviscid stability of this base flow, we seek a linear disturbance field of the form

$$(\tilde{u}, \tilde{v}, \tilde{w}, \tilde{p}) \exp[\mathrm{i}(\alpha X - \omega T)]. \tag{36}$$

As usual, this disturbance is on a short length scale (X) which is comparable to the local boundary-layer thickness, and a corresponding fast timescale T such that $(x, t) = \mathrm{Re}^{-\frac{1}{2}}(X, T)$. At leading order this leads to the following inviscid disturbance equations:

$$\mathrm{i}\alpha\tilde{u} + \tilde{v}_Y + \tilde{w}_Z = 0, \tag{37a}$$

$$\mathrm{i}\alpha(\hat{U} - \omega/\alpha)\tilde{u} + \tilde{v}\hat{U}_Y + \tilde{w}\hat{U}_Z = -\mathrm{i}\alpha\tilde{p}, \tag{37b}$$

$$\mathrm{i}\alpha(\hat{U} - \omega/\alpha)\tilde{v} = -\tilde{p}_Y, \tag{37c}$$

$$\mathrm{i}\alpha(\hat{U} - \omega/\alpha)\tilde{w} = -\tilde{p}_Z. \tag{37d}$$

The temperature profile remains decoupled resulting in a local Rayleigh problem, thermal effects would only remain coupled if $\mathrm{G} \gg 1$ as described by Hall [22]. By eliminating in favour of the disturbance pressure, and by considering a local wave number $\bar{\alpha}$ and frequency $\bar{\omega}$ of

$$\alpha = \left(\frac{n+1}{2}\right)^{\frac{1}{2}} x^{\frac{n-1}{2}}\bar{\alpha} \quad \text{and} \quad \omega = \left(\frac{n+1}{2}\right)^{\frac{1}{2}} x^{\frac{3n-1}{2}}\bar{\omega}, \tag{38}$$

we reduce (37) to

$$(\bar{\nabla}^2 - \bar{\alpha}^2)\tilde{p} = \frac{2}{U - \bar{\omega}/\bar{\alpha}}[U_\eta\, \tilde{p}_\eta + U_\zeta\, \tilde{p}_\zeta]. \tag{39}$$

To obtain this form we have moved to the coordinates (η, ζ) (9d) that describe the streak base state, where $\hat{U}(x, Y, Z) = x^n U(x, \eta, \zeta)$. This is the Rayleigh pressure equation, see for example Hall and Horseman [23] or Hewitt and Duck [24], and spatially unstable modes have $\bar{\alpha}_i \neq 0$. In the (η, ζ) far-field the disturbance pressure decays to $\tilde{p} = 0$, and on the plate $(\eta = 0)$ we have $\tilde{p}_\eta = 0$ by (37c). Varicose modes have symmetric (about $\zeta = 0$) $\tilde{p}$ whilst sinuous modes have antisymmetric $\tilde{p}$.

To solve the bi-global polynomial eigenvalue problem (39), we employ a second-order finite difference scheme for $\tilde{p}$, including $\bar{\alpha}$ as an extra degree of freedom. To compensate for the extra degree of freedom we must also apply an extra constraint on the system: we arbitrarily normalise the eigenfunctions so that $\tilde{p} = 1$ at a fixed node in the domain. This approach can only determine one eigenmode at a time, but avoids working with the full polynomial (in $\bar{\alpha}$) nature of (39). Initial guesses to the bi-global inviscid modes are taken from the corresponding viscous problem.

In Fig. 5, the $\mathrm{G} = 8$, 16 solutions each become unstable to a Rayleigh mode downstream, with the $\mathrm{G} = 16$ streak immediately exhibiting a sinuous instability at the heated region. We indicate approximate locations at which further instabilities are first exhibited: a sinuous mode for $\mathrm{G} = 8$ (plus-sign); and a varicose mode for $\mathrm{G} = 16$ (circle). Sinuous modes are found at lower values of the metric $\mathcal{A}$ than varicose modes.

The downstream evolution of the peak inviscid growth rate is shown in Fig. 7 using $\max_{\bar{\omega}}[-\bar{\alpha}_i]$, the spatial growth of the most unstable mode. The unstable points in Fig. 5 correspond to the lowest streamwise location of the unstable modes given in Fig. 7. The $G = 16$ streak is seen to be already unstable to a sinuous mode at the heated region.

The increased forcing associated with $\mathrm{G} = 16$ results in strongly nonlinear streak-like behaviour in the immediate vicinity of the heated region $(x = x_0)$, where unstable sinuous modes are found. The sinuous mode of the $\mathrm{G} = 16$ streak is consistently more unstable than the varicose mode. For weaker forcing with $\mathrm{G} = 8$, growth ultimately results in a nonlinear streak further downstream that is also unstable to an inviscid mode.

We depict the unstable sinuous and varicose modes of the $\mathrm{G} = 16$ streak in Fig. 8 at ad hoc choices of $x = 250$ and frequency $\bar{\omega} = 0.25$. Also shown is the upwards deflection of the streamwise velocity contours induced by the perturbation applied at $x = x_0 = 10$; only a truncated version of the larger computation domain is shown.

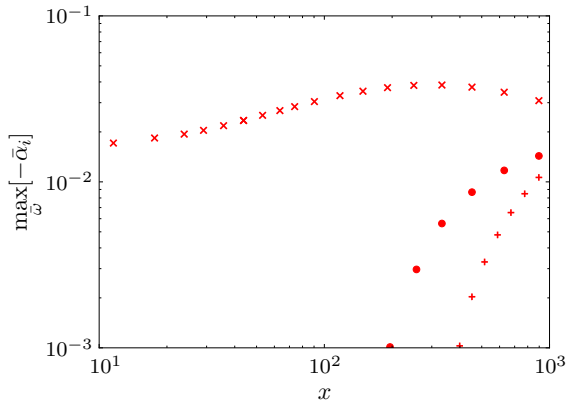

Fig. 7 The maximum exponential growth rate $-\bar{\alpha}_i$ for secondary instabilities of the G = 8, 16 streaks shown in Fig. 5. Sinuous modes develop for the G = 8 (plus signs) and G = 16 (crosses) streaks closer to the heated region than varicose modes. The G = 16 streak develops varicose modes in the given region (circles), whereas none are expressed for the G = 8 streak. Here the base flow is a nonlinear streak embedded in a Blasius boundary layer ($\beta = 0$) with Prandtl number Pr = 0.71

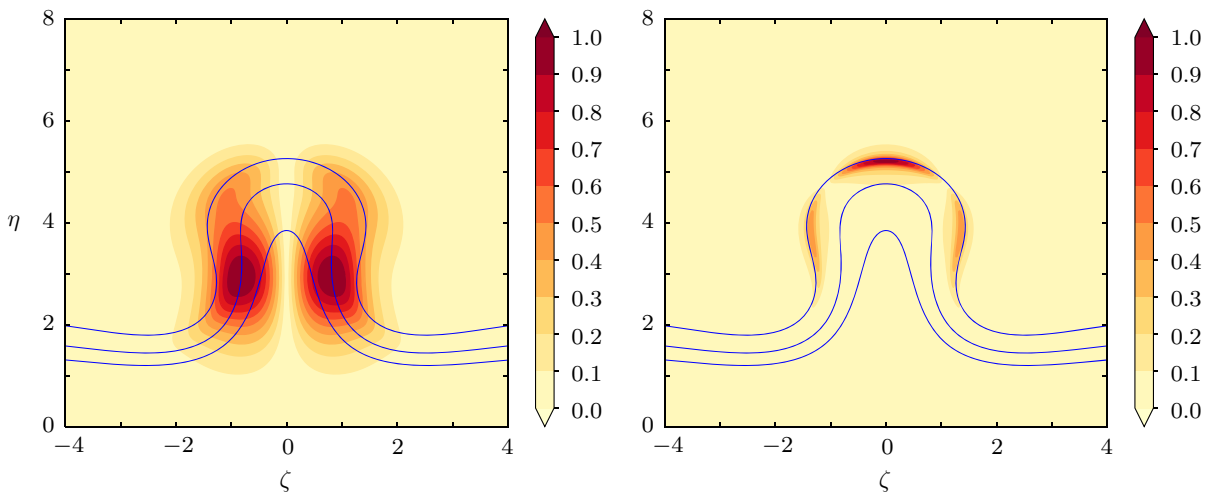

Fig. 8 The absolute streamwise velocity $|\tilde{u}|$ of sinuous (left) and varicose (right) perturbation eigenmodes determined at $x = 250$ for Grashof parameter G = 16 with $\bar{\omega} = 0.25$. Contours of the base flow streamwise velocity $\hat{U} = 0.7, 0.8, 0.9$ are overlaid in blue and the eigenmodes are normalised with $\max|\tilde{u}| = 1$. The corresponding eigenvalues are $\bar{\alpha} = 0.28 - 0.024i$ for the sinuous mode and $\bar{\alpha} = 0.28 - 0.0029i$ for the varicose mode. Here we have no applied pressure gradient ($\beta = 0$) and Pr = 0.71

The inviscid modes are comparable to those determined by Hall and Horseman [23] in the isothermal case for Görtler vortices and those of Andersson et al. [21] for boundary-layer streaks. This is to be expected as the qualitative downstream structure of our thermally induced streaks is comparable, and the inviscid disturbances remain decoupled from thermal effects.

5 Discussion

We have examined the Falkner–Skan flow over a flat plate, where the plate is subjected to a localised heating on a spanwise scale of $O(\mathrm{Re}^{-1/2})$; the simplest way to achieve this is via a localised surface temperature 'hot spot' such as (34). The Grashof number based on the peak hot spot temperature is assumed to be $O(\mathrm{Re}^{3/2})$ and this is sufficient to provide buoyancy forcing of the transverse momentum within the boundary layer. In Sect. 3,

we have determined the solution downstream of such a localised hot spot, showing that the perturbation to the streamwise velocity grows algebraically as x^{λ} ($\lambda > 0$) when the thermal forcing remains weak (Fig. 5). The linear form of the downstream algebraically growing disturbance is obtained directly in Sect. 2 via an eigenproblem. For stronger forcing, or equivalently further downstream, the perturbation amplitude becomes comparable to the two-dimensional boundary-layer base flow and a three-dimensional nonlinear streak is obtained (Fig. 8). In this strongly nonlinear regime the streak has been shown to be inviscidly unstable to Rayleigh waves (Figs. 7 and 8), which grow exponentially downstream with growth rate $O(\mathrm{Re}^{1/2})$. Hence, even modest localised temperature perturbations can force a streak response that will ultimately break down. Whilst a localised hot spot with a two-dimensional (x, Z dependent) heating of the type considered here has not been studied experimentally, Dovgal et al. [25] (for example) studied the influence of spanwise uniform heating near the leading edge so similar approaches could be applied here.

The form of the downstream algebraically growing disturbance is obtained using a bi-global eigenvalue computation, for which the non-parallel development of the modes is captured by similarity variables for the transverse and spanwise coordinates. The dominant eigenmode for the Blasius boundary layer in air (Prandtl number $\mathrm{Pr} \approx 0.71$) has $\lambda_1 \approx 0.203$ and the corresponding eigenfunction is as given in Fig. 1a in the cross section. This predicted growth rate of the bi-global eigenvalue problem is in agreement with that obtained in the nonlinear non-self-similar computations of Sect. 3 (Fig. 5) in the linear regime.

The self-similar nature of the eigenvalue problem can also be preserved if the plate is heated at all positions such that its temperature is $x^{3(n-1)/2}$, which introduces a (redefined) scaled Grashof parameter (G) based on the bulk plate temperature. Whilst this restricted spatial dependence is of limited practical interest, we note that even in this case, the eigenvalue spectrum is only weakly affected for $\mathrm{G} = O(1)$ (Table 1). For any plate temperatures that decay slower than this, we would expect the mechanism of Hall and Morris [16] to dominate.

For small Grashof parameter $\mathrm{G} \ll 1$, the bi-global eigenvalue spectrum can be obtained by a one-dimensional eigenvalue problem arising from the $k \ll 1$ Fourier transform of the energy equation (17); k being the spanwise wavenumber in the transformed solution. This one-dimensional eigenvalue problem can be used to efficiently determine the most dangerous spatial growth/decay $\lambda = \lambda_1$ over the full (β–Pr) parameter space, where β is the Hartree parameterisation of the external pressure gradient.

For any Prandtl number, there exists a growing eigenmode embedded in a Blasius boundary layer with $\beta = 0$ (Fig. 3). The spatial growth in this case is bounded between $0 < \lambda_1 < 0.25$. At more general values of $\beta > 0$ (a Falkner–Skan boundary layer with a favourable pressure gradient) the downstream growth (λ_1) is reduced and above a critical value we obtain decay with $\lambda_1 < 0$. For air, the dominant spatial growth λ_1 remains positive provided that the pressure gradient is less than $\beta \approx 0.183$.

The eigenproblem can also be examined for adverse pressure gradients ($\beta < 0$). In the case of $-0.1988 < \beta < 0$, it is known [26] that the Falkner–Skan equation (8c) has two branches, which are differentiated by the sign of $\tau = F''(\eta = 0)$. As expected, the application of an adverse pressure gradient increases the spatial growth of the eigenmodes. As a representative example, with pressure gradient $\beta = -0.1$, $\mathrm{Pr} = 0.71$, the dominant thermal mode has spatial growth $\lambda_1 = 0.307$ for the non-reversed ($\tau > 0$) Falkner–Skan boundary layer.

Appendix A: The full nonlinear (non-self-similar) marching problem

Nonlinear streamwise marching is undertaken to determine the steady response to a localised wall heating in Sect. 3. To capture the nonlinear downstream development of these flows, we must solve a parabolic problem that can be obtained from the steady form of (6) via the substitution (9a) and change of coordinate (9d).

We replace the cross-sectional velocities with

$$V = \frac{1-n}{1+n}\eta U(x,\eta,\zeta) - \Phi(x,\eta,\zeta), \quad W = \frac{1-n}{1+n}\zeta U(x,\eta,\zeta) - \Psi(x,\eta,\zeta), \tag{40}$$

and cross differentiate the corresponding momentum equations to eliminate the pressure in favour of a cross-sectional vorticity $\Theta = \Psi_\eta - \Phi_\zeta$. Furthermore, we explicitly extract the standard two-dimensional solution by the substitution

$$U = U_B(\eta) + \bar{U}(x,\eta,\zeta), \quad \Phi = \Phi_B(\eta) + \bar{\Phi}(x,\eta,\zeta), \quad \Psi = \zeta\Psi_B(\eta) + \bar{\Psi}(x,\eta,\zeta), \tag{41}$$

$$\Theta = \Theta_B(\eta) + \bar{\Theta}(x,\eta,\zeta), \quad \vartheta = \vartheta_B(\eta) + \bar{\vartheta}(x,\eta,\zeta), \tag{42}$$

where in terms of (8) this corresponds to $U_B = F'$, $\Psi_B = (1-\beta)F'$, $\Phi_B = F$, $\Theta_B = (1-\beta)F''$ and $\vartheta_B = H$.

The resulting parabolic system is

$$0 = (2-\beta)(x\bar{U}_x + \bar{U}) - \bar{\Phi}_\eta - \bar{\Psi}_\zeta, \tag{43a}$$

$$\bar{\Theta} = \bar{\Psi}_\eta - \bar{\Phi}_\zeta, \tag{43b}$$

$$\begin{aligned}\bar{U}_{\eta\eta} + \bar{U}_{\zeta\zeta} &= \beta[2U_B\bar{U} + \bar{U}^2] + (2-\beta)[U_B + \bar{U}]x\bar{U}_x \\ &\quad - (\Phi_B + \bar{\Phi})\bar{U}_\eta - (\zeta\Psi_B + \bar{\Psi})\bar{U}_\zeta - U_B'\bar{\Phi},\end{aligned} \tag{43c}$$

$$\begin{aligned}\bar{\Theta}_{\eta\eta} + \bar{\Theta}_{\zeta\zeta} &= 2(1-\beta)[\zeta(U_B + \bar{U})\bar{U}_\eta + \zeta U_B'\bar{U} - \eta(U_B + \bar{U})\bar{U}_\zeta] \\ &\quad - (\Phi_B + \bar{\Phi})\bar{\Theta}_\eta - \zeta\Theta_B'\bar{\Phi} - \zeta\Psi_B\bar{\Theta}_\zeta - \bar{\Psi}(\Theta_B + \bar{\Theta}_\zeta) \\ &\quad - (2-\beta)\left[(U_B + \bar{U})\bar{\Theta} + \zeta\Theta_B\bar{U} + (\zeta\Theta_B + \bar{\Theta})x\bar{U}_x\right] \\ &\quad + (2-\beta)x[(U_B' + \bar{U}_\eta)\bar{\Psi}_x + (U_B + \bar{U})\bar{\Theta}_x - \bar{U}_\zeta\bar{\Phi}_x] - G(2-\beta)^{\frac{3}{2}}\bar{\vartheta}_\zeta,\end{aligned} \tag{43d}$$

$$\begin{aligned}\frac{1}{\mathrm{Pr}}(\bar{\vartheta}_{\eta\eta} + \bar{\vartheta}_{\zeta\zeta}) &= (2-\beta)x(U_B + \bar{U})\bar{\vartheta}_x - (\Phi_B + \bar{\Phi})\bar{\vartheta}_\eta - (\zeta\Psi_B + \bar{\Psi})\bar{\vartheta}_\zeta \\ &\quad - \bar{\Phi}\vartheta'_B - 3(1-\beta)\left[(U_B + \bar{U})\bar{\vartheta} + \bar{U}\vartheta_B\right],\end{aligned} \tag{43e}$$

using the Hartree parameter $\beta = 2n/(n+1)$ for the applied pressure gradient.

Note that the linear eigenproblem defined by (11) is obtained from (43) by assuming that

$$(\bar{\Phi}, \bar{\Psi}, \bar{\Theta}, \bar{U}) = \epsilon x^\lambda(\tilde{\Phi}, \tilde{\Psi}, \tilde{\Theta}, \tilde{U}), \tag{44}$$

in the limit of $\epsilon \ll 1$.

References

1. Libby P, Fox H (1963) Some perturbation solutions in laminar boundary-layer theory. J Fluid Mech 17:433–449
2. Stewartson K (1957) On asymptotic expansions in the theory of boundary layers. J Math Phys 36(1–4):173–191
3. Schneider W, Wasel MG (1985) Breakdown of the boundary-layer approximation for mixed convection above a horizontal plate. Int J Heat Mass Transf 28(12):2307–2313
4. Wickern G (1991) Mixed convection from an arbitrarily inclined semi-infinite flat plate—I. The influence of the inclination angle. Int J Heat Mass Transf 34(8):1935–1945
5. Wickern G (1991) Mixed convection from an arbitrarily inclined semi-infinite flat plate—II. The influence of the Prandtl number. Int J Heat Mass Transf 34(8):1947–1957
6. Daniels PG (1992) A singularity in thermal boundary-layer flow on a horizontal surface. J Fluid Mech 242:419–440

7. Steinrück H (1994) Mixed convection over a cooled horizontal plate: non-uniqueness and numerical instabilities of the boundary-layer equations. J Fluid Mech 278:251–265
8. Denier JP, Duck PW, Li J (2005) On the growth (and suppression) of very short-scale disturbances in mixed forced-free convection boundary layers. J Fluid Mech 526:147–170
9. Luchini P (1996) Reynolds-number-independent instability of the boundary layer over a flat surface. J Fluid Mech 327:101–116
10. Duck PW, Stow SR, Dhanak MR (1999) Non-similarity solutions to the corner boundary-layer equations (and the effects of wall transpiration). J Fluid Mech 400:125–162
11. Hall P (2021) Long wavelength streamwise vortices caused by wall curvature or roughness. J Eng Math 128:2
12. Hewitt RE, Duck PW (2018) Localised streak solutions for a Blasius boundary layer. J Fluid Mech 849:885–901
13. Hewitt RE, Duck PW (2014) Three-dimensional boundary layers with short spanwise scales. J Fluid Mech 756:452–469
14. Falkner VM, Skan SW (1930) Some approximate solutions of the boundary layer equations. Philos Mag 12:865–896
15. Hartree DR (1937) On an equation occurring in Falkner and Skan's approximate treatment of the equations of the boundary layer. Math Proc Camb Philos Soc 33:223–239
16. Hall P, Morris H (1992) On the instability of boundary layers on heated flat plates. J Fluid Mech 245:367–400
17. Williams AJ, Hewitt RE (2017) Micro-slot injection into a boundary layer driven by a favourable pressure gradient. J Eng Math 107:19–35
18. Hernandez V, Roman JE, Vidal V (2005) SLEPc: a scalable and flexible toolkit for the solution of eigenvalue problems. ACM Trans Math Softw 31(3):351–362
19. Abramowitz M, Stegun IA (1972) Handbook of mathematical functions with formulas, graphs, and mathematical tables, 10th edn. US GPO, US Department of Commerce, Washington, DC
20. Balay S, Gropp WD, McInnes LC, Smith BF (1997) Efficient management of parallelism in object oriented numerical software libraries. In: Arge E, Bruaset AM, Langtangen HP (eds) Modern software tools in scientific computing. Birkhäuser, Boston, pp 163–202
21. Andersson P, Brandt P, Bottaro L, Henningson DS (2001) On the breakdown of boundary layer streaks. J Fluid Mech 428:29–60
22. Hall P (1993) Streamwise vortices in heated boundary layers. J Fluid Mech 252:301–324
23. Hall P, Horseman NJ (1991) The linear inviscid secondary instability of longitudinal vortex structures in boundary layers. J Fluid Mech 232:357–375
24. Hewitt RE, Duck PW (2019) Instability of isolated boundary-layer streaks to spatially-developing travelling waves. Eur J Mech B Fluids 76:413–421
25. Dovgal AV, Levchenko VY, Timofeev VA (1990) Boundary layer control by a local heating of the wall. In: Laminar–turbulent transition. Springer, Berlin, pp 131–121
26. Stewartson K (1954) Further solutions of the Falkner–Skan equation. Math Proc Camb Philos Soc 50:454–465